ACS APPLIED MATERIALS & INTERFACES

Research Article

Cite This: ACS Appl. Mater. Interfaces 2019, 11, 3372−3381

www.acsami.org

Reaction Packaging $CoSe_2$ Nanoparticles in N-Doped Carbon Polyhedra with Bifunctionality for Overall Water Splitting

Hengyi Lu,[†,‡] Youfang Zhang,[†] Yunpeng Huang,[‡] Chao Zhang,*[,†] and Tianxi Liu*[,†,‡]

[†]State Key Laboratory for Modification of Chemical Fibers and Polymer Materials, College of Materials Science and Engineering, Innovation Center for Textile Science and Technology, Donghua University, Shanghai 201620, P. R. China

[‡]State Key Laboratory of Molecular Engineering of Polymers, Department of Macromolecular Science, Fudan University, Shanghai 200433, P. R. China

Supporting Information

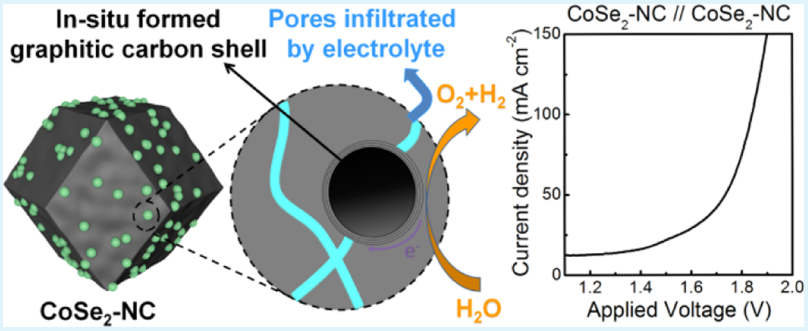

ABSTRACT: Water electrolysis is a promising approach for green and large-scale hydrogen production; however, there are still challenges for developing efficient and stable bifunctional electrocatalysts toward the hydrogen and oxygen evolution reactions. Herein, zeolitic imidazolate framework-67 was used as the precursor for the construction of $CoSe_2$ nanoparticles trapped in N-doped carbon (NC) polyhedra. Among as-obtained $CoSe_2$-NC hybrid, highly active $CoSe_2$ nanoparticles in sizes of 10−20 nm are encapsulated in N-doped few-layer carbon shell, avoiding their easy aggregations of $CoSe_2$ nanoparticles as well as enhancing the long-term stability. The unique nanostructured $CoSe_2$-NC hybrid with a hierarchical porosity and 3D conductive framework thus fully exerts outstanding bifunctional catalytic activity of $CoSe_2$ centers. As a result, the $CoSe_2$-NC hybrid as bifunctional catalysts for overall water splitting delivers a high current density of 50 mA cm^{-2} with an applied voltage of ∼1.73 V in an alkaline electrolyte, with a promising stability over 50 000 s.

KEYWORDS: *ZIF67, selenide reaction, carbon polyhedra, bifunctional electrocatalyst, overall water splitting*

1. INTRODUCTION

Developing clean and renewable alternatives to fossil fuels is a matter of great urgency.[1−3] Among various of alternatives, hydrogen is regarded as most promising clean energy carriers because of its high energy density and environmentally friendly features.[1,4,5] Water electrolysis is the most efficient and large-scale strategy for the simultaneous production of hydrogen and oxygen.[6,7] The water electrolysis is composed of two basic reactions, namely, the hydrogen evolution reaction (HER) and oxygen evolution reaction (OER).[8] The sluggish kinetics of the two reactions greatly hinder energy conversion efficiency for overall water splitting.[7,9−11] Therefore, the development of efficient and durable bifunctional HER/OER catalysts is the key to achieve high energy efficiency for an electrolyzer. An ideal electrocatalyst for overall water splitting demands to generate high and stable electrocatalytic current at a low overpotential for long-term operation. Up to now, Pt-group metals and Ir-/Ru-based compounds are the efficient HER and OER electrocatalysts, respectively, for commercial uses. The shortcomings of low reserves and high costs of these precious metal-based materials have greatly limited their practical and large-scale applications.[8]

Great efforts have been made toward the development of low-cost, high-performance, and long-durability HER and OER electrocatalysts. Varieties of transition-metal compounds are utilized as the promising electrocatalysts for HER (metal oxides, metal sulfides, phosphides, carbides/nitrides, etc.)[12−24] and OER (metal oxides, hydroxides, perovskite, nitrides, chalcogenides, etc.).[25−32] Among these transition-metal compounds, cobaltous selenide ($CoSe_2$) is expected to perform a remarkable HER and OER activity in both acid and alkaline electrolytes.[33,34] However, the $CoSe_2$ in the form of nanoparticles suffers from severe problems of easy aggregation and oxidation, which greatly impede efficient exposures of active centers and thus lead to the performance far below exception.[35−37] For example, the Xie group obtained an

Received: November 16, 2018
Accepted: December 26, 2018
Published: December 26, 2018

DOI: 10.1021/acsami.8b20184
ACS Appl. Mater. Interfaces 2019, 11, 3372−3381

outstanding OER performance by reducing the thickness of the $CoSe_2$ nanosheets into atomic scale, boosting the intrinsic high OER activity of $CoSe_2$.[38] Recently, encapsulations of active metal-based nanoparticles into carbon nanotubes or graphitic carbon shells have been developed as an efficient way to improve their electrochemical performance.[35,39−43] For instances, through encapsulating the iron, cobalt, and their alloys into N-doped carbon (NC) nanotubes via chemical vapor deposition, Deng et al. realized long-term highly active non-precious-metal catalysts in acid.[44] However, the uniform dispersion of the nanoparticle catalysts in interconnected carbon matrix via a simple and green strategy is still a great challenge.

Metal−organic framework (MOF) and its derived materials, possessing orderly structure, large surface area, high porosity, and controllable morphology, have attracted great attentions.[4,45] MOF-derived materials can be easily tailored by tuning the metal species within the MOF precursor or introducing additive components during post treatments.[46−50] The MOF-derived materials with hierarchical porous structure and controllable morphology guarantee exposures of more electrochemically active sites, beneficial for shorten ion diffusions of electrolytes.[51−54] Herein, we put forward a selenide reaction packaging strategy for preparation of $CoSe_2$ nanoparticles trapped in NC polyhedra using the zeolitic imidazolate framework-67 (ZIF67) as the precursor. Among the as-obtained $CoSe_2$-NC hybrid, $CoSe_2$ nanoparticles, wrapped by few-layer NC shells, are tightly anchored within the NC framework. The closely wrapped NC shells largely enhance long-term stability of the $CoSe_2$ core in alkaline electrolyte, and the NC framework with high graphitization degree and unique polyhedral morphology shows an integrated conductive network facilitating fast electron transfer during electrocatalysis. Simultaneously, the hierarchical porous structure of the NC framework ensures fully exposures of catalytic active centers in electrolytes. As a result, the as-obtained $CoSe_2$-NC hybrid performs outstanding bifunctional catalytic performance toward HER and OER in alkaline, delivering high water electrolytic current under low overpotential, with small Tafel slope and impressive long-term stability.

2. EXPERIMENTAL SECTION

2.1. Preparation of the ZIF67. The synthesis of ZIF67 was based on a previous method with a slight modification.[55,56] Basically, 4 mmol $Co(NO_3)_2$ was dissolved in 100 mL methanol and 16 mmol 2-methylimidazole was dissolved in another 100 mL of methanol. The above two solutions were mixed and maintained for 24 h below 5 °C. The sample was obtained by centrifugation, washing with methanol and drying at 80 °C overnight in a vacuum oven.

2.2. Preparation of the Co-NC Hybrid. The Co-NC hybrid was prepared by direct pyrolysis of ZIF67 in inert gas followed by acid leaching. Typically, the ZIF67 powder was put into a covered crucible and then heated to a certain temperature at a heating rate of 2 °C min^{-1} under 50 sccm Ar and kept for another 2 h before cooling down. The obtained sample was washed with a 0.5 M H_2SO_4 solution for 6 h, collected by centrifugation, and washed with water/ethanol before drying at 80 °C. The products obtained under 700, 800, and 900 °C were labeled as Co-NC-700, Co-NC-800, and Co-NC-900, respectively. The products prepared by the same method without acid leaching were labeled as Co-NC-700-W, Co-NC-800-W, and Co-NC-900-W.

2.3. Preparation of the $CoSe_2$-NC Hybrid. The $CoSe_2$-NC hybrid was prepared by gas-phase selenization reaction. Typically, the Co-NC-800 hybrid powder was first mixed with Se powder (mass ratio: Co-NC/Se = 2/1) by gridding. Then, the mixture powder was put into a covered crucible and then heated to a certain temperature for 2 h under 100 sccm Ar. The as-obtained black powder is the $CoSe_2$-NC hybrid. $CoSe_2$-NC-800 obtained under 350, 400, and 450 °C were labeled as $CoSe_2^{(350)}$-NC-800, $CoSe_2^{(400)}$-NC-800, and $CoSe_2^{(450)}$-NC-800, respectively (for instance, "$^{(350)}$" indicates that the selenization reaction temperature is 350 °C). The $CoSe_2$-NC-700 and $CoSe_2$-NC-900 hybrid were prepared by the same procedure by using the Co-NC-700 and Co-NC-900 as the precursor, respectively.

3. RESULTS AND DISCUSSION

The ZIF67 precursor was first prepared as the precursor for the synthesis of the $CoSe_2$-NC hybrid. Figure S1 exhibits the SEM images of the as-prepared ZIF67, which have a rhombic dodecahedral morphology with a smooth surface and uniform size of ∼500 nm. The X-ray diffraction (XRD) pattern confirms good crystallinity of the as-obtained ZIF67 (Figure S2). The schematic of the synthesis of the $CoSe_2$-NC hybrid is illustrated in Figure 1. In the first step, the Co nanoparticles

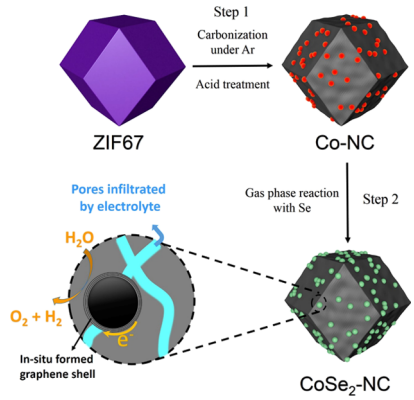

Figure 1. Schematic of the preparation of the $CoSe_2$ nanoparticles trapped in NC polyhedra ($CoSe_2$-NC) hybrid.

trapped in the NC (Co-NC) were obtained by direct pyrolysis of ZIF67 followed by acid leaching. Compared with traditional methods for preparation of metal/carbon hybrids, the approach using the ZIF67 as the precursor has many advantages such as convenience, easy to obtain uniformly distributed metal nanoparticles, and so on.[57,58] SEM images of pyrolyzed products obtained at 800 °C (Co-NC-800-W) are shown in Figure S3. The Co-NC-800-W sample inherits a polyhedron structure but shows a rough surface and slightly reduced size. The Co-NC-800 hybrid obtained by washing the Co-NC-800-W in acid possesses a similar polyhedron structure of the Co-NC-800-W (Figure 2a,b). Transmission electron microscopy (TEM) image of the Co-NC-800 (Figure 2c) reveals that Co nanoparticles are uniformly encapsulated in 3D porous carbon framework with small sizes. The Co nanoparticles are surrounded with few-layer carbon shells, which are in situ grown during pyrolysis because of a catalytic carbonization property of in situ formed metallic Co.[59,60] The acid-leaching treatment efficiently created more pores inside the NC framework by removing unstable Co nanoparticles, thus achieving high surface area and excellent electrochemical performance (Figures S4 and S5). The acid-leaching condition is optimized to be a 0.5 M H_2SO_4 solution (related discussions in Figures S6 and S7). Upon acid-leaching, most of remained Co nanoparticles were closely wrapped by in situ formed few-layer carbon shells, protecting Co cores from acid leaching.

DOI: 10.1021/acsami.8b20184
ACS Appl. Mater. Interfaces 2019, 11, 3372−3381

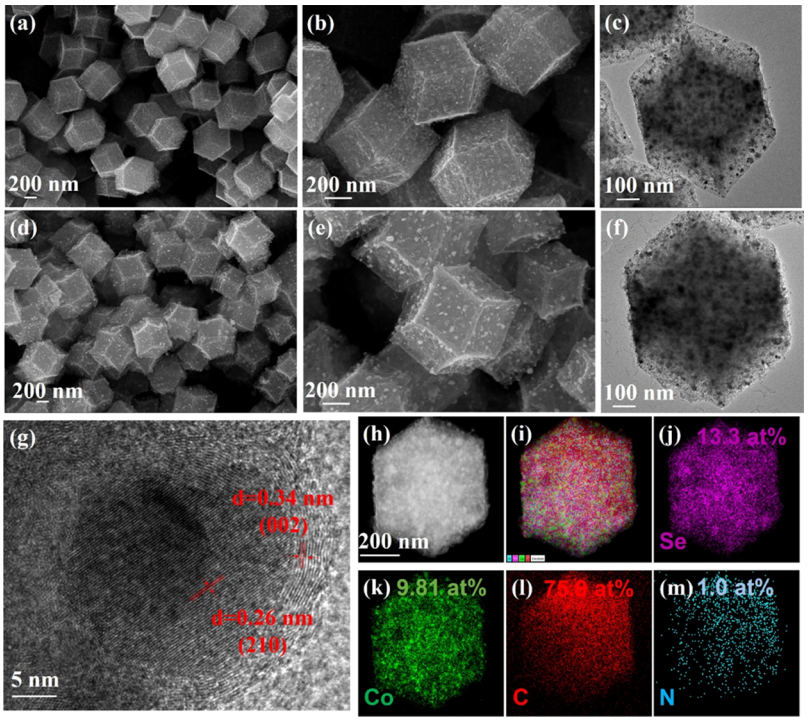

Figure 2. (a,b) SEM and (c) TEM images of the Co-NC-800, (d,e) SEM, (f) TEM, (g) high-resolution TEM, (h) STEM images of the $CoSe_2^{(400)}$-NC-800 with the EDXS mappings of (i) overlapped, (j) Se, (k) Co, (l) C, and (m) N elements.

In the second step, a selenization reaction packaging strategy was utilized for the conversion of the Co-NC hybrid into the $CoSe_2$ nanoparticles trapped in the NC ($CoSe_2$-NC). Upon selenization reaction at 400 °C, the $CoSe_2^{(400)}$-NC-800 (Figure 2d–f) shows a rough and porous structure, and uniform distributions of $CoSe_2$ nanoparticles are well maintained. The detailed microstructure of the hybrid was further characterized by high-resolution TEM (Figure 2g). The $CoSe_2$ nanoparticles are closely wrapped by few-layer carbon shells. Besides, the lattice spacing of the graphitic shells and $CoSe_2$ cores are ~0.34 and 0.26 nm, respectively, which are corresponding to the (002) crystalline plane of graphitic carbon and (210) crystalline plane of $CoSe_2$, respectively, confirming the successful conversion of metallic Co into $CoSe_2$. During the selenization, in situ formed $CoSe_2$ nanoparticles are confined in few-layer carbon shells, thus avoiding self-agglomerations. A series of the $CoSe_2$-NC hybrids are obtained by tailoring the preparation parameters, thus realizing an optimization. The scanning TEM (STEM) and energy-dispersive X-ray spectroscopy (EDXS) mappings of the $CoSe_2^{(400)}$-NC-800 reveal the uniform distributions of the C, N, Co, and Se elements within the hybrids (Figure 2h–m).

XRD characterizations were conducted to investigate the chemical components and crystalline structures in the Co-NC-800 and $CoSe_2^{(400)}$-NC-800 (Figure 3a). For the Co-NC-800, two diffraction patterns at 44.3 and 51.6° correspond to (111) and (200) crystalline planes of metallic Co (JCPDS no. 15-0806), and the broad XRD pattern at 25.8° is assigned to the (002) facet of graphitic carbon. The $CoSe_2^{(400)}$-NC-800 sample shows characteristic diffraction patterns of $CoSe_2$ (JCPDS no. 53-0449), confirming the successful formation of $CoSe_2$. The diffraction pattern at 44.3° in the $CoSe_2^{(400)}$-NC-800 indicates that the metallic Co form is maintained in some nanoparticles. These "nonconvertible" Co nanoparticles are totally inactive and can be ignored in the $CoSe_2^{(400)}$-NC-800 hybrid because they are densely covered by thick carbon shell and could not react with Se gas as well as electrolytic ions for further reactions. X-ray spectroscopy (XPS) measurements reveal that the $CoSe_2^{(400)}$-NC-800 mainly consists of C, O, Co, N, and Se elements. The presence of N 1s region indicates the nitrogen doping of the carbon matrix, which could enhance the electrochemical performance of the hybrid materials.[61] High-resolution Se 3d and Co 2p spectra in Figure 3c,d confirm the formation of $CoSe_2$ within the hybrid.[62,63] Nitrogen adsorption/desorption tests were applied to investigate the pore structure evolutions before and after the selenization reaction. From Figure 3e, the isotherm curves of the Co-NC-800 and $CoSe_2^{(400)}$-NC-800 belong to typical type-IV isotherms, demonstrating the existence of mesopores in these two samples. The Brunauer–Emmet–Teller-specific surface areas of the Co-NC-800 and $CoSe_2^{(400)}$-NC-800 are 279 and 295 $m^2\ g^{-1}$, respectively. The pore size distributions of these samples are plotted by a Barrett–Joyner–Halenda method. For Figure 3f, the Co-NC-800 and $CoSe_2^{(400)}$-NC-800 show similar pore size distributions, indicating the coexistences of micropores and mesopores in the samples. These results imply that the gas-phase selenization reaction causes no obvious changes of pore structures, indicating that the hierarchical porous structure of the Co-NC is well maintained during the selenization.

To optimize the temperatures for the selenization reaction, the $CoSe_2$-NC-800 samples obtained under different selenization temperatures of 350 and 450 °C were also synthesized. The morphological results indicate that both $CoSe_2^{(350)}$-NC-800 and $CoSe_2^{(450)}$-NC-800 (Figure 4) maintain regular porous structure of the Co-NC-800. However, the sizes of imbedded $CoSe_2$ nanoparticles increase with the increase of selenization temperatures, and the particle sizes of the $CoSe_2$ within the $CoSe_2^{(350)}$-NC-800, $CoSe_2^{(400)}$-NC-800, and $CoSe_2^{(450)}$-NC-800 are in the ranges of 12–17, 14–28, and

DOI: 10.1021/acsami.8b20184
ACS Appl. Mater. Interfaces 2019, 11, 3372–3381

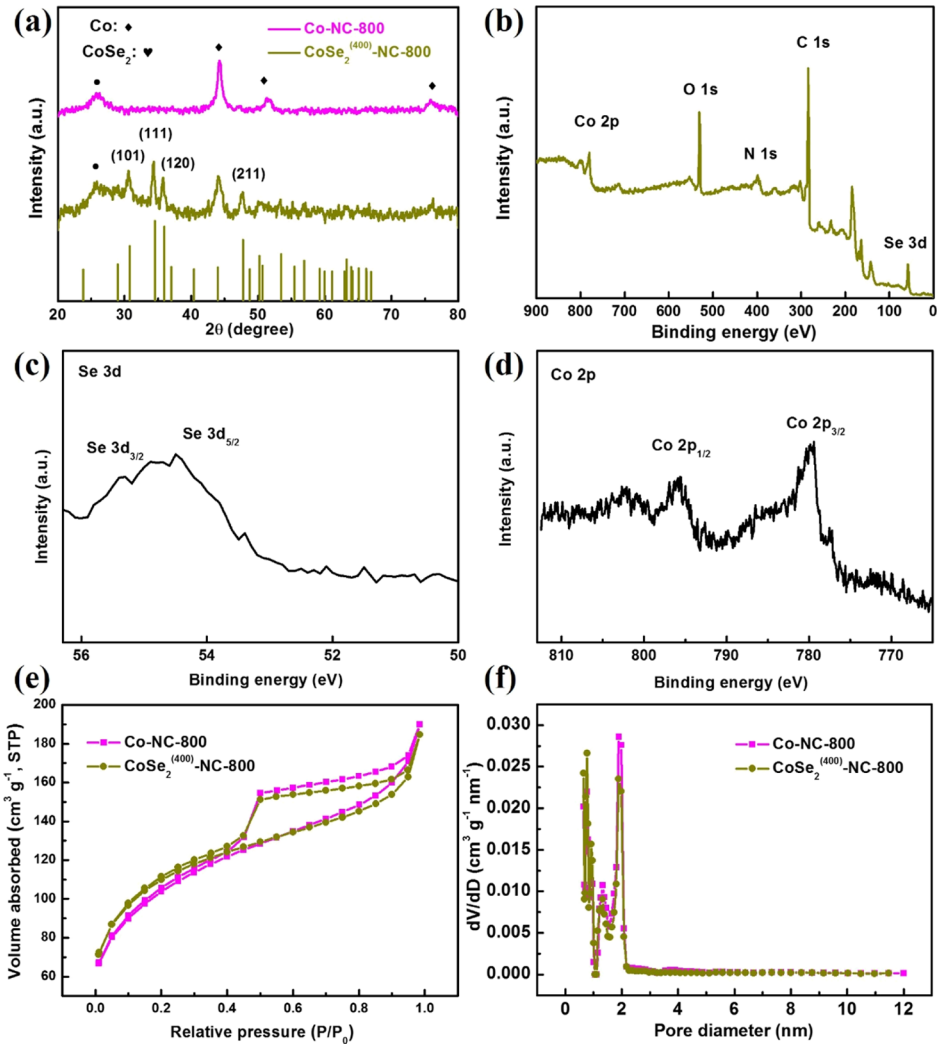

Figure 3. (a) XRD patterns of the Co-NC-800 and $CoSe_2^{(400)}$-NC-800. (b) XPS survey, (c) Se 3d, and (d) Co 2p spectra of the $CoSe_2^{(400)}$-NC-800. (e) Nitrogen adsorption/desorption isotherms and (f) pore size distributions of the Co-NC-800 and $CoSe_2^{(400)}$-NC-800.

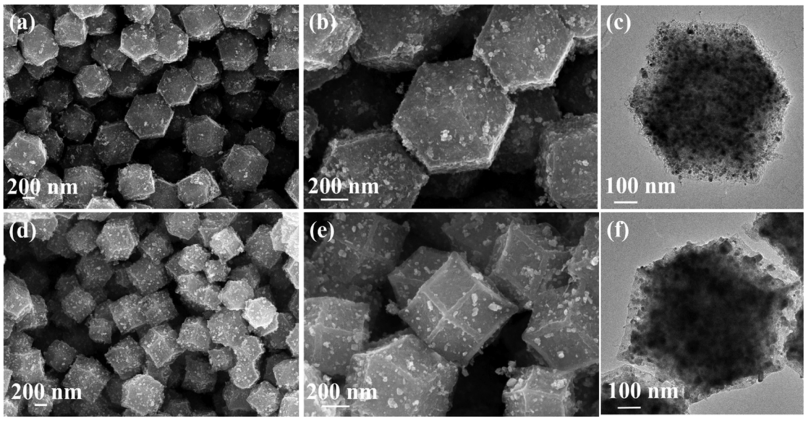

Figure 4. SEM and TEM images of (a–c) $CoSe_2^{(350)}$-NC-800 and (d–f) $CoSe_2^{(450)}$-NC-800.

47–57 nm, respectively. The sizes of the $CoSe_2$ nanoparticles would greatly affect exposed active site number of the $CoSe_2$-NC hybrid, which would in turn affect the electrochemical performance of the catalyst.

The electrocatalytic HER performance of different samples was evaluated by recording their linear sweep voltammetry (LSV) curves at a scan rate of 2 mV s^{-1} in a N_2-saturated 0.5 M H_2SO_4. Figure 5a shows the LSV curves of different samples without *iR* compensations. The commercial Pt/C catalyst shows the highest onset potential as well as lowest Tafel slope, as expected. All the $CoSe_2$-NC-800 catalysts show improved HER performance compared with the Co-NC-800, indicating their much higher activities of embedded $CoSe_2$ than that of Co nanoparticles. Among the $CoSe_2$-NC-800 catalysts

DOI: 10.1021/acsami.8b20184
ACS Appl. Mater. Interfaces 2019, 11, 3372–3381

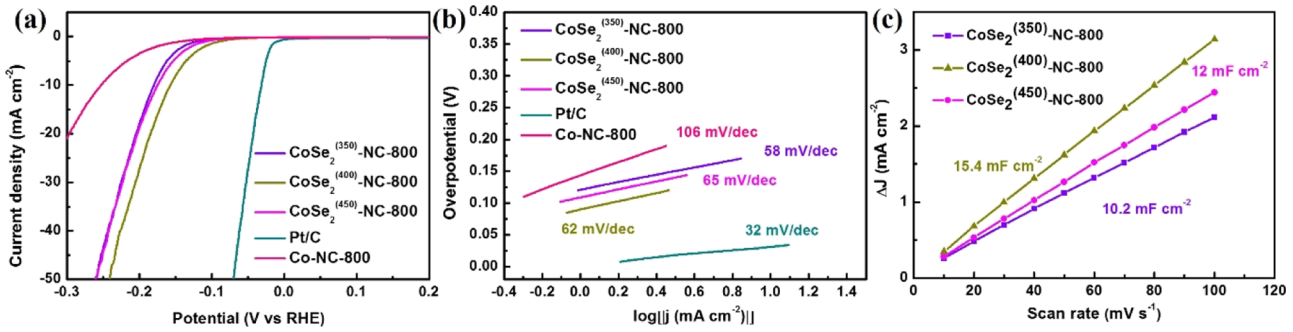

Figure 5. (a) LSV curves and (b) Tafel plots of the $CoSe_2$-NC-800 at different selenization temperatures, Co-NC-800, and Pt/C in 0.5 M H_2SO_4. (c) C_{dl} of the $CoSe_2$-NC-800 obtained at different selenization temperatures.

obtained by different selenization temperatures, the $CoSe_2^{(400)}$-NC-800 sample exhibits the lowest onset potential (−84 mV) and the potential reaching a current density of 10 mA cm^{-2} (−156 mV), revealing its better HER performance than the $CoSe_2^{(350)}$-NC-800 (−181 mV at 10 mA cm^{-2}) and $CoSe_2^{(450)}$-NC-800 (−175 mV at 10 mA cm^{-2}). The Tafel slopes of the $CoSe_2$-NC-800 catalysts vary from 58 to 65 mV dec^{-1}, suggesting that the HER processes of the $CoSe_2$-NC hybrid undergoes a Volmer−Heyrovesky pathway. As discussed in the Experimental Section, the selenization temperature would affect the $CoSe_2$ particle sizes among the hybrid, which would definitely cause effects on the electrochemical active surface area (ECSA) of the catalysts. Therefore, the C_{dl} of different $CoSe_2$-NC-800 samples were determined by collecting their cyclic voltammetry (CV) curves under scan rates from 10 to 100 mV s^{-1} in non-Faradaic regions to reflect their ECSA (Figure S8). From Figure 5c, the $CoSe_2^{(400)}$-NC-800 catalyst possesses a higher C_{dl} of 15.4 mF cm^{-2} than that of $CoSe_2^{(350)}$-NC-800 (12 mF cm^{-2}) and $CoSe_2^{(450)}$-NC-800 (10.2 mF cm^{-2}), indicating that the $CoSe_2$-NC-800 obtained at a selenization temperature of 400 °C has the largest ECSA. Larger ECSA means more active sites at solid−liquid interfaces during electrocatalysis, thus helping to achieve better catalytic performance.

Furthermore, the carbonization temperature of the ZIF67 precursor was also optimized. Figure 6 shows the $CoSe_2^{(400)}$-NC hybrid prepared from the Co-NC-700 and Co-NC-900. Both $CoSe_2^{(400)}$-NC-700 and $CoSe_2^{(400)}$-NC-900 show the similar polyhedron-like morphology and small particle sizes of the $CoSe_2$ like the $CoSe_2^{(400)}$-NC-800, expect that some macropores appear in the carbon framework of the $CoSe_2^{(400)}$-NC-900. These macropores were created by acid leaching of large-sized Co nanoparticles formed under high calcination temperature (Figures S9 and S10). TEM images (Figures 2c and S10e) show that the contents of Co nanoparticles in the Co-NC-900 are significantly less than that of the Co-NC-800. This is because higher calcination temperature would increase the contents of large-sized Co nanoparticles that are easier to be removed upon acid treatment, thus leaving only a small quantity of small-sized Co particles within leached products. Lower Co contents in the Co-NC samples consequently cause lower $CoSe_2$ contents within the $CoSe_2$-NC, proved by thermogravimetric analysis (TGA) results in Figure S11. The weight contents of the $CoSe_2$ nanoparticles in the $CoSe_2^{(400)}$-NC-700, $CoSe_2^{(400)}$-NC-800, and $CoSe_2^{(400)}$-NC-900 are 68.7, 47.9, and 10.2%, respectively. Raman measurements were used to reveal the differences of the graphitic degrees and electrical conductivities of related samples.[64] In Figure S12, the I_D/I_G ratios of Raman spectra decrease when increasing the pyrolytic temperatures, indicating that higher graphitic degrees as well as higher electrical conductivity are obtained under higher pyrolytic temperature.

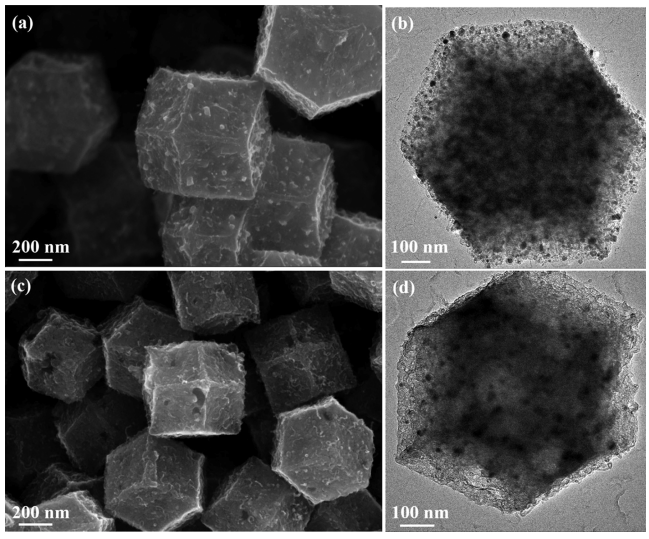

Figure 6. SEM and TEM images of (a,b) $CoSe_2^{(400)}$-NC-700 and (c,d) $CoSe_2^{(400)}$-NC-900.

Figure 7a indicates the LSV curves of different $CoSe_2^{(400)}$-NC hybrids in 0.5 M H_2SO_4. The optimized HER performance was obtained at the pyrolysis temperature of 800 °C. The carbonization temperature of the ZIF67 precursor is strongly related to the electrical conductivity of the carbon framework and the content of Co nanoparticles. When the carbonization temperature increases, the conductivity of the $CoSe_2^{(400)}$-NC hybrids gradually increases (reflected by decreased semicircle diameters in Figures 7c and S12), but the active site density decreases in the same time. An optimal balance of the amounts of active sites and electrical conductivities was realized at 800 °C, where an optimized electrochemical activity was obtained. TEM images of the $CoSe_2^{(400)}$-NC-800 catalysts after cycling for 50 000 s in 0.5 M H_2SO_4 show that the $CoSe_2^{(400)}$-NC-800 sample remains in the initial polyhedron shape after long-time cycling, and no obvious changes of the $CoSe_2$ nanoparticle in the carbon species can be observed, indicating the high stability of the $CoSe_2$ in acidic electrolytes for cycling (Figure S13).

The HER and OER performance of the $CoSe_2^{(400)}$-NC hybrid was then investigated in 1 M KOH electrolyte, and the commercial HER catalyst (Pt/C) and OER catalyst (IrO_2)

DOI: 10.1021/acsami.8b20184
ACS Appl. Mater. Interfaces 2019, 11, 3372−3381

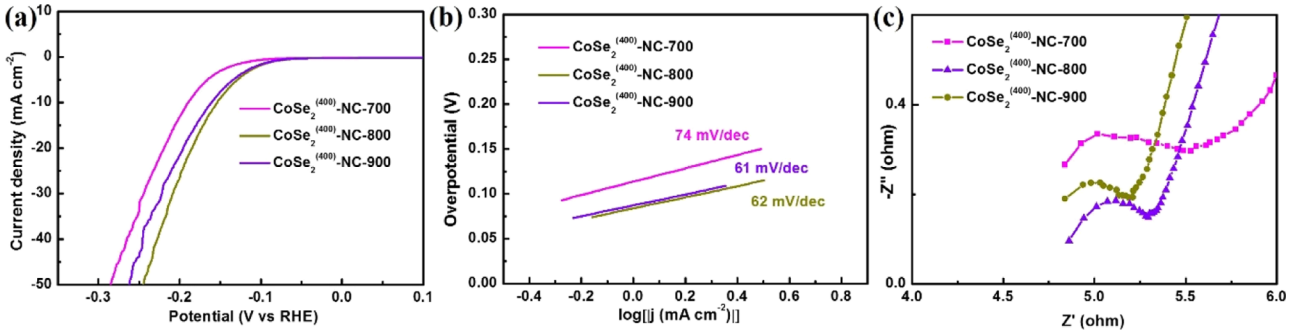

Figure 7. (a) LSV curves, (b) Tafel plots, and (c) Nyquist plots of the $CoSe_2^{(400)}$-NC hybrid obtained at different carbonization temperatures in 0.5 M H_2SO_4.

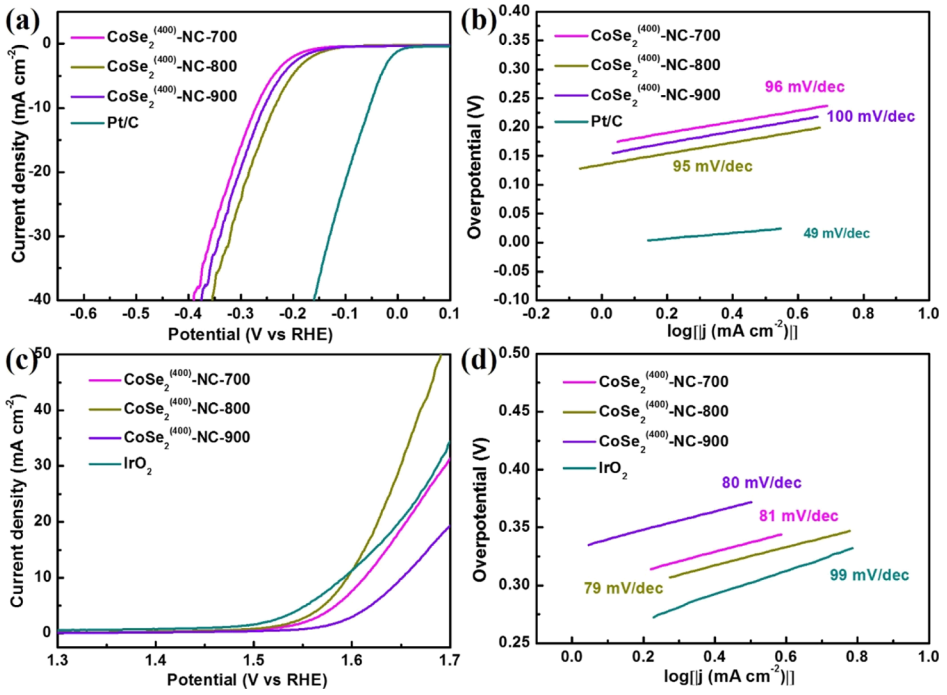

Figure 8. (a,b) HER and (c,d) OER performance of the $CoSe_2^{(400)}$-NC hybrid and corresponding commercial catalysts in 1 M KOH.

were also measured for comparison (Figure 8). The $CoSe_2^{(400)}$-NC-800 catalyst shows the best HER performance, exhibiting low onset potential of −125 mV, small Tafel slope of 95 mV dec^{-1}, and current density of 10 mA cm^{-2} at an overpotential of 234 mV. For the OER process, the onset potential of the $CoSe_2^{(400)}$-NC-800 is 1.535 V and a low potential of 1.59 V is needed to provide the current density of 10 mA cm^{-2}. The Tafel slope of the $CoSe_2^{(400)}$-NC-800, which is even lower than commercial IrO_2 catalyst, once again confirms its superior activity.

Cycling stability is an important property to judge a catalyst in its practical use. We characterized the cycling stability of the $CoSe_2^{(400)}$-NC-800 catalyst by recording the current−time curves at a fixed voltage. As shown in Figure 9a,b, the current density of the $CoSe_2^{(400)}$-NC-800 catalyst shows no obvious decreases after continuous operations for 50 000 s for the HER and OER, respectively, indicating its excellent cycling stability in basic electrolytes. The excellent cycling stability of the $CoSe_2^{(400)}$-NC-800 catalyst is derived from the unique structure of 3D carbon framework tethered $CoSe_2$ nanoparticles with a NC layer protection. In this hybrid, the $CoSe_2$ active centers are firmly encapsulated in few-layer NC shells, acting as protective layers alleviating damages of the $CoSe_2$ cores in strong alkali environments, thereby ensuring the long-term durability. The TEM−EDXS results of the $CoSe_2^{(400)}$-NC-800 catalyst after HER and OER cycling in 1 M KOH are shown in Figures S14 and S15. After cycling, the Se/Co atom ratio decreased and the new O elements appeared. This is because the surface of $CoSe_2$ nanoparticles may be slightly oxidized in alkaline electrolytes.[65] The above performance results show great potentials of the $CoSe_2^{(400)}$-NC-800 as a bifunctional catalyst for overall water splitting. As a demonstration, an alkaline electrolyzer using the $CoSe_2^{(400)}$-NC-800 as both cathode and anode catalysts was then constructed to assess its practical water splitting performance (digital image in Figure S16). As shown in Figure 9c, the $CoSe_2^{(400)}$-NC-800//$CoSe_2^{(400)}$-NC-800 electrolyzer exhibits outstanding water splitting performance, achieving the current density at 50 mA cm^{-2} with an applied voltage of only 1.73 V. The electrolyzer maintains extremely stable for more than 50 000 s with the current density larger than 40 mA cm^{-2}. However, as a control sample, neat Ni foam shows almost no water splitting current density even as high as 2.0 V. These results indicate that the $CoSe_2^{(400)}$-NC-800 can be used as a

DOI: 10.1021/acsami.8b20184
ACS Appl. Mater. Interfaces 2019, 11, 3372−3381

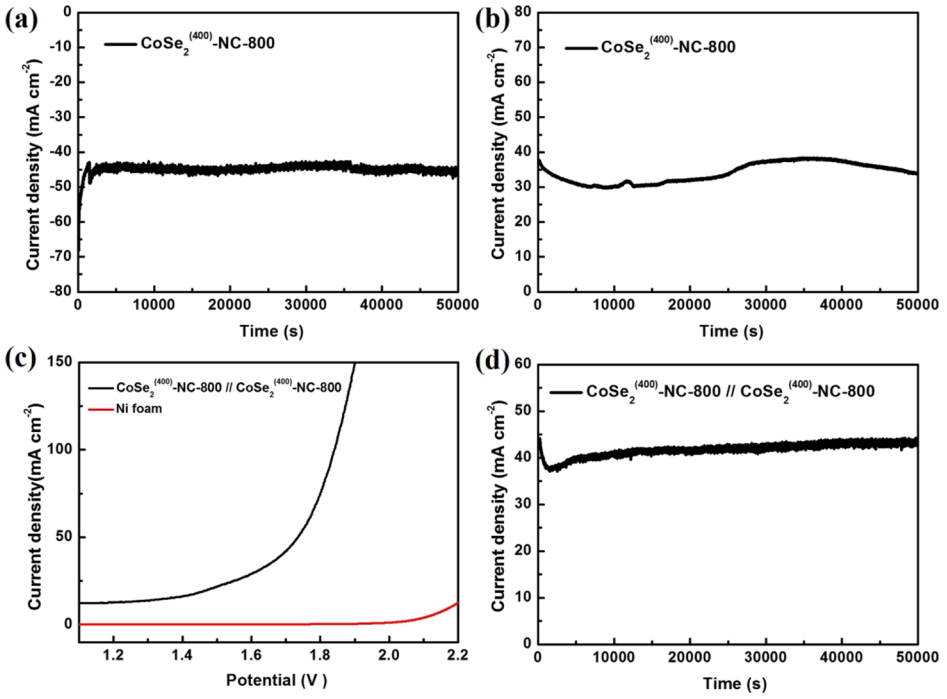

Figure 9. *I*–*t* curves for (a) HER and (b) OER of the $CoSe_2^{(400)}$-NC-800 in 1 M KOH. (c) LSV and (d) *i*–*t* curve of the $CoSe_2^{(400)}$-NC-800// $CoSe_2^{(400)}$-NC-800 electrolyzer for overall water splitting in 1 M KOH.

highly efficient and durable bifunctional catalyst in the overall water splitting, and its performance is highly competitive with the carbon hybrid catalysts in the literature (Table S1).

The outstanding performance of the $CoSe_2^{(400)}$-NC-800 is derived from its unique composition and nanostructure. First, the $CoSe_2$ nanoparticles obtained by in situ selenization from metallic Co nanoparticles have excellent catalytic activity and serve as catalytic active centers for the HER and OER. Second, the hierarchical porous carbon framework with large surface areas and plenty micro-/mesopores greatly enhance the interplay interfaces between the electrolytes and the active centers, ensuring full exposures of active $CoSe_2$. Third, highly conductive NC shells around the $CoSe_2$ core are not only beneficial for rapid electron transfer on catalytic active centers but also guarantee the electrochemical stability of the catalyst. All these factors working together therefore promote the catalytic performance of the $CoSe_2^{(400)}$-NC-800 as a bifunctional catalyst for overall water splitting.

4. CONCLUSION

In summary, we proposed a simple and efficient selenide reaction packaging strategy for the synthesis of the $CoSe_2$ nanoparticles trapped in NC polyhedra using ZIF67 as the precursor. The as-obtained $CoSe_2$-NC hybrid exhibits an outstanding bifunctional catalytic activity for the HER and OER. Beneficial from integrated porous structures and closely wrapped carbon shells on $CoSe_2$ active centers, the electrolyzer using the $CoSe_2$-NC hybrid as the anode and cathode shows an outstanding performance, delivering high current density of 50 mA cm^{-2} at a low potential of 1.73 V with a superior durability. We believe that this synthetic strategy can be extended for preparation of various carbon-based hybrid materials for future energy applications.

■ ASSOCIATED CONTENT

Supporting Information

The Supporting Information is available free of charge on the ACS Publications website at DOI: 10.1021/acsami.8b20184.

Experimental section including materials, characterization, electrochemical characterization; SEM images and XRD pattern of the ZIF67; SEM images of Co-NC-800-W; LSV curves and Tafel plots of Co-NC-800-W, Co-NC-800, $CoSe_2$-NC-800-W, and $CoSe_2$-NC-800 in 0.5 M H_2SO_4; SEM images of $CoSe_2$-NC-800-W; LSV curves of Co-NC-800 and $CoSe_2$-NC-800 by different acid-leaching conditions; SEM images of $CoSe_2$-NC-800 by different acid-leaching conditions; CV curves of $CoSe_2^{(350)}$-NC-800, $CoSe_2^{(400)}$-NC-800, and $CoSe_2^{(450)}$-NC-800; SEM images of Co-NC-700-W and Co-NC-700; TEM image of Co-NC-700; SEM images of Co-NC-900-W and Co-NC-900; TEM image of Co-NC-900; TGA curves of Co-NC-700, Co-NC-800, Co-NC-900, $CoSe_2^{(400)}$-NC-700, $CoSe_2^{(400)}$-NC-800, and $CoSe_2^{(400)}$-NC-900 in air; Raman spectra of the Co-NC-700, Co-NC-800, Co-NC-900, $CoSe_2^{(400)}$-NC-700, $CoSe_2^{(400)}$-NC-800, $CoSe_2^{(400)}$-NC-900; TEM images of $CoSe_2^{(400)}$-NC-800 after cycling; TEM, bright-field TEM, EDXS mappings of $CoSe_2^{(400)}$-NC-800 after cycling for HER and OER; digital image of the electrolyzer using Ni foam-loaded $CoSe_2^{(400)}$-NC-800 catalysts as both cathode and anode; and summary of the electrochemical parameters of the $CoSe_2$-NC with carbon hybrid materials for the overall water splitting in the literature (PDF)

(PDF)

■ AUTHOR INFORMATION

Corresponding Authors

*E-mail: czhang@dhu.edu.cn (C.Z.).

DOI: 10.1021/acsami.8b20184
ACS Appl. Mater. Interfaces 2019, 11, 3372–3381

*E-mail: txliu@fudan.edu.cn, txliu@dhu.edu.cn (T.L.).

ORCID

Chao Zhang: 0000-0003-1255-7183

Tianxi Liu: 0000-0002-5592-7386

Notes

The authors declare no competing financial interest.

■ ACKNOWLEDGMENTS

We are grateful for the financial support from the Fundamental Research Funds for the Central Universities (2232016A3-02), the National Natural Science Foundation of China (51433001, 21504012, and 51773035), the Program of Shanghai Subject Chief Scientist (17XD1400100), the Science and Technology Commission of Shanghai Municipality (16520722100), the Shanghai Rising-Star Program (18QA1400200), the Natural Science Foundation of Shanghai (17ZR1439900), and the Shanghai Scientific and Technological Innovation Project (18JC1410600).

■ REFERENCES

(1) Zou, X.; Zhang, Y. Noble Metal-Free Hydrogen Evolution Catalysts for Water Splitting. *Chem. Soc. Rev.* **2015**, *44*, 5148−5180.

(2) Wu, M.; Wang, Y.; Wei, Z.; Wang, L.; Zhuo, M.; Zhang, J.; Han, X.; Ma, J. Ternary doped porous carbon nanofibers with excellent ORR and OER performance for zinc-air batteries. *J. Mater. Chem. A* **2018**, *6*, 10918−10925.

(3) Xue, Z.-H.; Han, J.-T.; Feng, W.-J.; Yu, Q.-Y.; Li, X.-H.; Antonietti, M.; Chen, J.-S. Tuning the Adsorption Energy of Methanol Molecules Along Ni-N-Doped Carbon Phase Boundaries by the Mott-Schottky Effect for Gas-Phase Methanol Dehydrogenation. *Angew. Chem.* **2018**, *130*, 2727−2731.

(4) Wang, W.; Xu, X.; Zhou, W.; Shao, Z. Recent Progress in Metal-Organic Frameworks for Applications in Electrocatalytic and Photocatalytic Water Splitting. *Adv. Sci.* **2017**, *4*, 1600371.

(5) Jayaramulu, K.; Masa, J.; Tomanec, O.; Peeters, D.; Ranc, V.; Schneemann, A.; Zboril, R.; Schuhmann, W.; Fischer, R. A. Nanoporous Nitrogen-Doped Graphene Oxide/Nickel Sulfide Composite Sheets Derived From a Metal-Organic Framework as an Efficient Electrocatalyst for Hydrogen and Oxygen Evolution. *Adv. Funct. Mater.* **2017**, *27*, 1700451.

(6) Yoo, H. D.; Markevich, E.; Salitra, G.; Sharon, D.; Aurbach, D. On the Challenge of Developing Advanced Technologies for Electrochemical Energy Storage and Conversion. *Mater. Today* **2014**, *17*, 110−121.

(7) Anantharaj, S.; Ede, S. R.; Sakthikumar, K.; Karthick, K.; Mishra, S.; Kundu, S. Recent Trends and Perspectives in Electrochemical Water Splitting with an Emphasis On Sulfide, Selenide, and Phosphide Catalysts of Fe, Co, and Ni: A Review. *ACS Catal.* **2016**, *6*, 8069−8097.

(8) Wang, J.; Cui, W.; Liu, Q.; Xing, Z.; Asiri, A. M.; Sun, X. Recent Progress in Cobalt-Based Heterogeneous Catalysts for Electrochemical Water Splitting. *Adv. Mater.* **2015**, *28*, 215−230.

(9) Zhu, Y.; Chen, G.; Xu, X.; Yang, G.; Liu, M.; Shao, Z. Enhancing Electrocatalytic Activity for Hydrogen Evolution by Strongly Coupled Molybdenum Nitride@Nitrogen-Doped Carbon Porous Nano-Octahedrons. *ACS Catal.* **2017**, *7*, 3540−3547.

(10) Tabassum, H.; Guo, W.; Meng, W.; Mahmood, A.; Zhao, R.; Wang, Q.; Zou, R. Metal-Organic Frameworks Derived Cobalt Phosphide Architecture Encapsulated Into B/N Co-Doped Graphene Nanotubes for All pH Value Electrochemical Hydrogen Evolution. *Adv. Energy Mater.* **2017**, *7*, 1601671.

(11) Yan, L.; Cao, L.; Dai, P.; Gu, X.; Liu, D.; Li, L.; Wang, Y.; Zhao, X. Metal-Organic Frameworks Derived Nanotube of Nickel-Cobalt Bimetal Phosphides as Highly Efficient Electrocatalysts for Overall Water Splitting. *Adv. Funct. Mater.* **2017**, *27*, 1703455.

(12) Yu, Z.; Bai, Y.; Liu, Y.; Zhang, S.; Chen, D.; Zhang, N.; Sun, K. Metal-Organic-Framework-Derived Yolk-Shell-Structured Cobalt-Based Bimetallic Oxide Polyhedron with High Activity for Electrocatalytic Oxygen Evolution. *ACS Appl. Mater. Interfaces* **2017**, *9*, 31777−31785.

(13) Tian, J.; Liu, Q.; Asiri, A. M.; Sun, X. Self-Supported Nanoporous Cobalt Phosphide Nanowire Arrays: An Efficient 3D Hydrogen-Evolving Cathode over the Wide Range of pH 0-14. *J. Am. Chem. Soc.* **2014**, *136*, 7587−7590.

(14) Popczun, E. J.; McKone, J. R.; Read, C. G.; Biacchi, A. J.; Wiltrout, A. M.; Lewis, N. S.; Schaak, R. E. Nanostructured Nickel Phosphide as an Electrocatalyst for the Hydrogen Evolution Reaction. *J. Am. Chem. Soc.* **2013**, *135*, 9267−9270.

(15) Kong, D.; Wang, H.; Lu, Z.; Cui, Y. $CoSe_2$ Nanoparticles Grown on Carbon Fiber Paper: An Efficient and Stable Electrocatalyst for Hydrogen Evolution Reaction. *J. Am. Chem. Soc.* **2014**, *136*, 4897−4900.

(16) Tang, C.; Cheng, N.; Pu, Z.; Xing, W.; Sun, X. NiSe Nanowire Film Supported On Nickel Foam: An Efficient and Stable 3D Bifunctional Electrode for Full Water Splitting. *Angew. Chem.* **2015**, *127*, 9483−9487.

(17) Liao, L.; Zhu, J.; Bian, X.; Zhu, L.; Scanlon, M. D.; Girault, H. H.; Liu, B. MoS_2 Formed on Mesoporous Graphene as a Highly Active Catalyst for Hydrogen Evolution. *Adv. Funct. Mater.* **2013**, *23*, 5326−5333.

(18) Liu, Y.; Yu, G.; Li, G.-D.; Sun, Y.; Asefa, T.; Chen, W.; Zou, X. Coupling Mo_2C with Nitrogen-Rich Nanocarbon Leads to Efficient Hydrogen-Evolution Electrocatalytic Sites. *Angew. Chem.* **2015**, *127*, 10902−10907.

(19) Wu, H. B.; Xia, B. Y.; Yu, L.; Yu, X.-Y.; Lou, X. W. Porous Molybdenum Carbide Nano-Octahedrons Synthesized Via Confined Carburization in Metal-Organic Frameworks for Efficient Hydrogen Production. *Nat. Commun.* **2015**, *6*, 6512.

(20) Chen, W.-F.; Muckerman, J. T.; Fujita, E. Recent Developments in Transition Metal Carbides and Nitrides as Hydrogen Evolution Electrocatalysts. *Chem. Commun.* **2013**, *49*, 8896−8909.

(21) Ma, J.; Wang, M.; Lei, G.; Zhang, G.; Zhang, F.; Peng, W.; Fan, X.; Li, Y. Polyaniline Derived N-Doped Carbon-Coated Cobalt Phosphide Nanoparticles Deposited On N-Doped Graphene as an Efficient Electrocatalyst for Hydrogen Evolution Reaction. *Small* **2017**, *14*, 1702895.

(22) Zhang, J.-Y.; Wang, H.; Tian, Y.; Yan, Y.; Xue, Q.; He, T.; Liu, H.; Wang, C.; Chen, Y.; Xia, B. Y. Anodic Hydrazine Oxidation Assists Energy-Efficient Hydrogen Evolution Over a Bifunctional Cobalt Perselenide Nanosheet Electrode. *Angew. Chem.* **2018**, *130*, 7775−7779.

(23) Su, H.; Wang, H.-H.; Zhang, B.; Wang, K.-X.; Li, X.-H.; Chen, J.-S. Enriching Co nanoparticles inside carbon nanofibers via nanoscale assembly of metal-organic complexes for highly efficient hydrogen evolution. *Nano Energy* **2016**, *22*, 79−86.

(24) Xue, Z.-H.; Su, H.; Yu, Q.-Y.; Zhang, B.; Wang, H.-H.; Li, X.-H.; Chen, J.-S. Janus Co/CoP Nanoparticles as Efficient Mott-Schottky Electrocatalysts for Overall Water Splitting in Wide pH Range. *Adv. Energy Mater.* **2017**, *7*, 1602355.

(25) Hutchings, G. S.; Zhang, Y.; Li, J.; Yonemoto, B. T.; Zhou, X.; Zhu, K.; Jiao, F. In Situ Formation of Cobalt Oxide Nanocubanes as Efficient Oxygen Evolution Catalysts. *J. Am. Chem. Soc.* **2015**, *137*, 4223−4229.

(26) Long, X.; Li, J.; Xiao, S.; Yan, K.; Wang, Z.; Chen, H.; Yang, S. A Strongly Coupled Graphene and FeNi Double Hydroxide Hybrid as an Excellent Electrocatalyst for the Oxygen Evolution Reaction. *Angew. Chem.* **2014**, *126*, 7714−7718.

(27) Jung, J.-I.; Jeong, H. Y.; Lee, J.-S.; Kim, M. G.; Cho, J. A Bifunctional Perovskite Catalyst for Oxygen Reduction and Evolution. *Angew. Chem.* **2014**, *126*, 4670−4674.

(28) Xu, K.; Chen, P.; Li, X.; Tong, Y.; Ding, H.; Wu, X.; Chu, W.; Peng, Z.; Wu, C.; Xie, Y. Metallic Nickel Nitride Nanosheets Realizing Enhanced Electrochemical Water Oxidation. *J. Am. Chem. Soc.* **2015**, *137*, 4119−4125.

DOI: 10.1021/acsami.8b20184
ACS Appl. Mater. Interfaces 2019, 11, 3372−3381

(29) Liu, Y.; Cheng, H.; Lyu, M.; Fan, S.; Liu, Q.; Zhang, W.; Zhi, Y.; Wang, C.; Xiao, C.; Wei, S.; Ye, B.; Xie, Y. Low Overpotential in Vacancy-Rich Ultrathin $CoSe_2$ Nanosheets for Water Oxidation. *J. Am. Chem. Soc.* **2014**, *136*, 15670−15675.
(30) Lu, F.; Zhou, M.; Zhou, Y.; Zeng, X. First-Row Transition Metal Based Catalysts for the Oxygen Evolution Reaction Under Alkaline Conditions: Basic Principles and Recent Advances. *Small* **2017**, *13*, 1701931.
(31) Zhang, J.-Y.; Tian, X.; He, T.; Zaman, S.; Miao, M.; Yan, Y.; Qi, K.; Dong, Z.; Liu, H.; Xia, B. Y. In situ formation of Ni_3Se_4 nanorod arrays as versatile electrocatalysts for electrochemical oxidation reactions in hybrid water electrolysis. *J. Mater. Chem. A* **2018**, *6*, 15653−15658.
(32) Lv, L.-B.; Ye, T.-N.; Gong, L.-H.; Wang, K.-X.; Su, J.; Li, X.-H.; Chen, J.-S. Anchoring Cobalt Nanocrystals through the Plane of Graphene: Highly Integrated Electrocatalyst for Oxygen Reduction Reaction. *Chem. Mater.* **2015**, *27*, 544−549.
(33) Kwak, I. H.; Im, H. S.; Jang, D. M.; Kim, Y. W.; Park, K.; Lim, Y. R.; Cha, E. H.; Park, J. $CoSe_2$ and $NiSe_2$ Nanocrystals as Superior Bifunctional Catalysts for Electrochemical and Photoelectrochemical Water Splitting. *ACS Appl. Mater. Interfaces* **2016**, *8*, 5327−5334.
(34) Kim, J. K.; Park, G. D.; Kim, J. H.; Park, S.-K.; Kang, Y. C. Rational Design and Synthesis of Extremely Efficient Macroporous $CoSe_2$-CNT Composite Microspheres for Hydrogen Evolution Reaction. *Small* **2017**, *13*, 1700068.
(35) Wang, X.; Li, F.; Li, W.; Gao, W.; Tang, Y.; Li, R. Hollow bimetallic cobalt-based selenide polyhedrons derived from metal-organic framework: an efficient bifunctional electrocatalyst for overall water splitting. *J. Mater. Chem. A* **2017**, *5*, 17982−17989.
(36) Gao, M.-R.; Cao, X.; Gao, Q.; Xu, Y.-F.; Zheng, Y.-R.; Jiang, J.; Yu, S.-H. Nitrogen-Doped Graphene Supported $CoSe_2$ Nanobelt Composite Catalyst for Efficient Water Oxidation. *ACS Nano* **2014**, *8*, 3970−3978.
(37) Li, S.; Peng, S.; Huang, L.; Cui, X.; Al-Enizi, A. M.; Zheng, G. Carbon-Coated Co^{3+}-Rich Cobalt Selenide Derived from ZIF-67 for Efficient Electrochemical Water Oxidation. *ACS Appl. Mater. Interfaces* **2016**, *8*, 20534−20539.
(38) Liu, Y.; Cheng, H.; Lyu, M.; Fan, S.; Liu, Q.; Zhang, W.; Zhi, Y.; Wang, C.; Xiao, C.; Wei, S.; Ye, B.; Xie, Y. Low Overpotential in Vacancy-Rich Ultrathin $CoSe_2$ Nanosheets for Water Oxidation. *J. Am. Chem. Soc.* **2014**, *136*, 15670−15675.
(39) Xu, Y.; Tu, W.; Zhang, B.; Yin, S.; Huang, Y.; Kraft, M.; Xu, R. Nickel Nanoparticles Encapsulated in Few-Layer Nitrogen-Doped Graphene Derived from Metal-Organic Frameworks as Efficient Bifunctional Electrocatalysts for Overall Water Splitting. *Adv. Mater.* **2017**, *29*, 1605957.
(40) Wang, J.; Wu, H.; Gao, D.; Miao, S.; Wang, G.; Bao, X. High-density iron nanoparticles encapsulated within nitrogen-doped carbon nanoshell as efficient oxygen electrocatalyst for zinc-air battery. *Nano Energy* **2015**, *13*, 387−396.
(41) Wang, X.; Huang, X.; Gao, W.; Tang, Y.; Jiang, P.; Lan, K.; Yang, R.; Wang, B.; Li, R. Metal-organic framework derived $CoTe_2$ encapsulated in nitrogen-doped carbon nanotube frameworks: a high-efficiency bifunctional electrocatalyst for overall water splitting. *J. Mater. Chem. A* **2018**, *6*, 3684−3691.
(42) Zeng, M.; Liu, Y.; Zhao, F.; Nie, K.; Han, N.; Wang, X.; Huang, W.; Song, X.; Zhong, J.; Li, Y. Metallic Cobalt Nanoparticles Encapsulated in Nitrogen-Enriched Graphene Shells: Its Bifunctional Electrocatalysis and Application in Zinc-Air Batteries. *Adv. Funct. Mater.* **2016**, *26*, 4397−4404.
(43) Su, H.; Zhang, K.-X.; Zhang, B.; Wang, H.-H.; Yu, Q.-Y.; Li, X.-H.; Antonietti, M.; Chen, J.-S. Activating Cobalt Nanoparticles via the Mott-Schottky Effect in Nitrogen-Rich Carbon Shells for Base-Free Aerobic Oxidation of Alcohols to Esters. *J. Am. Chem. Soc.* **2017**, *139*, 811−818.
(44) Deng, J.; Ren, P.; Deng, D.; Yu, L.; Yang, F.; Bao, X. Highly Active and Durable Non-Precious-Metal Catalysts Encapsulated in Carbon Nanotubes for Hydrogen Evolution Reaction. *Energy Environ. Sci.* **2014**, *7*, 1919−1923.
(45) Wang, H.; Zhu, Q.-L.; Zou, R.; Xu, Q. Metal-Organic Frameworks for Energy Applications. *Chem* **2017**, *2*, 52−80.
(46) Wei, J.; Hu, Y.; Wu, Z.; Liang, Y.; Leong, S.; Kong, B.; Zhang, X.; Zhao, D.; Simon, G. P.; Wang, H. A graphene-directed assembly route to hierarchically porous Co-Nx/C catalysts for high-performance oxygen reduction. *J. Mater. Chem. A* **2015**, *3*, 16867−16873.
(47) Jiang, Z.; Lu, W.; Li, Z.; Ho, K. H.; Li, X.; Jiao, X.; Chen, D. Synthesis of Amorphous Cobalt Sulfide Polyhedral Nanocages for High Performance Supercapacitors. *J. Mater. Chem. A* **2014**, *2*, 8603−8606.
(48) Xu, M.; Han, L.; Han, Y.; Yu, Y.; Zhai, J.; Dong, S. Porous CoP concave polyhedron electrocatalysts synthesized from metal-organic frameworks with enhanced electrochemical properties for hydrogen evolution. *J. Mater. Chem. A* **2015**, *3*, 21471−21477.
(49) Wu, J.; Song, Y.; Zhou, R.; Chen, S.; Zuo, L.; Hou, H.; Wang, L. Zn-Fe-ZIF-derived porous $ZnFe_2O_4$/C@NCNT nanocomposites as anodes for lithium-ion batteries. *J. Mater. Chem. A* **2015**, *3*, 7793−7798.
(50) Wang, Q.; Zou, R.; Xia, W.; Ma, J.; Qiu, B.; Mahmood, A.; Zhao, R.; Yang, Y.; Xia, D.; Xu, Q. Facile Synthesis of Ultrasmall CoS_2 Nanoparticles within Thin N-Doped Porous Carbon Shell for High Performance Lithium-Ion Batteries. *Small* **2015**, *11*, 2511−2517.
(51) Jiao, L.; Zhou, Y.-X.; Jiang, H.-L. Metal-organic framework-based CoP/reduced graphene oxide: high-performance bifunctional electrocatalyst for overall water splitting. *Chem. Sci.* **2016**, *7*, 1690−1695.
(52) Liu, S.; Wang, Z.; Zhou, S.; Yu, F.; Yu, M.; Chiang, C.-Y.; Zhou, W.; Zhao, J.; Qiu, J. Metal-Organic-Framework-Derived Hybrid Carbon Nanocages as a Bifunctional Electrocatalyst for Oxygen Reduction and Evolution. *Adv. Mater.* **2017**, *29*, 1700874.
(53) Chen, L.; Chen, X.; Liu, H.; Li, Y. Encapsulation of Mono- or Bimetal Nanoparticles Inside Metal-Organic Frameworks via In situ Incorporation of Metal Precursors. *Small* **2015**, *11*, 2642−2648.
(54) Yan, Y.; He, T.; Zhao, B.; Qi, K.; Liu, H.; Xia, B. Y. Metal/covalent-organic frameworks-based electrocatalysts for water splitting. *J. Mater. Chem. A* **2018**, *6*, 15905−15926.
(55) You, B.; Jiang, N.; Sheng, M.; Gul, S.; Yano, J.; Sun, Y. High-Performance Overall Water Splitting Electrocatalysts Derived from Cobalt-Based Metal-Organic Frameworks. *Chem. Mater.* **2015**, *27*, 7636−7642.
(56) Shao, J.; Wan, Z.; Liu, H.; Zheng, H.; Gao, T.; Shen, M.; Qu, Q.; Zheng, H. Metal organic frameworks-derived Co_3O_4 hollow dodecahedrons with controllable interiors as outstanding anodes for Li storage. *J. Mater. Chem. A* **2014**, *2*, 12194−12200.
(57) Shen, K.; Chen, X.; Chen, J.; Li, Y. Development of MOF-Derived Carbon-Based Nanomaterials for Efficient Catalysis. *ACS Catal.* **2016**, *6*, 5887−5903.
(58) Mahmood, A.; Guo, W.; Tabassum, H.; Zou, R. Metal-Organic Framework-Based Nanomaterials for Electrocatalysis. *Adv. Energy Mater.* **2016**, *6*, 1600423.
(59) Hou, Y.; Li, J.; Wen, Z.; Cui, S.; Yuan, C.; Chen, J. Co_3O_4 nanoparticles embedded in nitrogen-doped porous carbon dodecahedrons with enhanced electrochemical properties for lithium storage and water splitting. *Nano Energy* **2015**, *12*, 1−8.
(60) Tu, Y.; Li, H.; Deng, D.; Xiao, J.; Cui, X.; Ding, D.; Chen, M.; Bao, X. Low Charge Overpotential of Lithium-Oxygen Batteries with Metallic Co Encapsulated in Single-Layer Graphene Shell as the Catalyst. *Nano Energy* **2016**, *30*, 877−884.
(61) Zhou, W.; Jia, J.; Lu, J.; Yang, L.; Hou, D.; Li, G.; Chen, S. Recent Developments of Carbon-Based Electrocatalysts for Hydrogen Evolution Reaction. *Nano Energy* **2016**, *28*, 29−43.
(62) Lee, C.-P.; Chen, W.-F.; Billo, T.; Lin, Y.-G.; Fu, F.-Y.; Samireddi, S.; Lee, C.-H.; Hwang, J.-S.; Chen, K.-H.; Chen, L.-C. Beaded stream-like $CoSe_2$ nanoneedle array for efficient hydrogen evolution electrocatalysis. *J. Mater. Chem. A* **2016**, *4*, 4553−4561.
(63) Wang, K.; Xi, D.; Zhou, C.; Shi, Z.; Xia, H.; Liu, G.; Qiao, G. $CoSe_2$ necklace-like nanowires supported by carbon fiber paper: a 3D integrated electrode for the hydrogen evolution reaction. *J. Mater. Chem. A* **2015**, *3*, 9415−9420.

DOI: 10.1021/acsami.8b20184
ACS Appl. Mater. Interfaces 2019, 11, 3372−3381

(64) Wang, L.; Wang, Y.; Wu, M.; Wei, Z.; Cui, C.; Mao, M.; Zhang, J.; Han, X.; Liu, Q.; Ma, J. Nitrogen, Fluorine, and Boron Ternary Doped Carbon Fibers as Cathode Electrocatalysts for Zinc-Air Batteries. *Small* **2018**, *14*, 1800737.
(65) Gu, C.; Hu, S.; Zheng, X.; Gao, M.-R.; Zheng, Y.-R.; Shi, L.; Gao, Q.; Zheng, X.; Chu, W.; Yao, H.-B.; Zhu, J.; Yu, S.-H. Synthesis of Sub-2 nm Iron-Doped $NiSe_2$ Nanowires and Their Surface-Confined Oxidation for Oxygen Evolution Catalysis. *Angew. Chem., Int. Ed.* **2018**, *57*, 4020−4024.

DOI: 10.1021/acsami.8b20184
ACS Appl. Mater. Interfaces 2019, 11, 3372−3381